JTTEE5 25:494–508
DOI: 10.1007/s11666-015-0354-8
1059-9630/$19.00 © ASM International

Peer Reviewed

Thermal Spray Using a High-Frequency Pulse Detonation Combustor Operated in the Liquid-Purge Mode

T. Endo, R. Obayashi, T. Tajiri, K. Kimura, Y. Morohashi, T. Johzaki, K. Matsuoka, T. Hanafusa, and S. Mizunari

(Submitted June 1, 2015; in revised form September 22, 2015)

Experiments on thermal spray by pulsed detonations at 150 Hz were conducted. Two types of pulse detonation combustors were used, one operated in the inert gas purge (GAP) mode and the other in the liquid-purge (LIP) mode. In both modes, all gases were supplied in the valveless mode. The GAP mode is free of moving components, although the explosive mixture is unavoidably diluted with the inert gas used for the purge of the hot burned gas. In the LIP mode, pure fuel-oxygen combustion can be realized, although a liquid-droplet injector must be actuated cyclically. The objective of this work was to demonstrate a higher spraying temperature in the LIP mode. First, the temperature of CoNiCrAlY particles heated by pulsed detonations was measured. As a result, the spraying temperature in the LIP mode was higher than that in the GAP mode by about 1000 K. Second, the temperature of yttria-stabilized zirconia (YSZ) particles, whose melting point was almost 2800 °C, heated by pulsed detonations in the LIP mode was measured. As a result, the YSZ particles were heated up to about 2500 °C. Finally, a thermal spray experiment using YSZ particles was conducted, and a coating with low porosity was successfully deposited.

Keywords CoNiCrAlY, detonation, liquid-purge mode, zirconia

1. Introduction

A detonation is a supersonic combustion wave where a leading shock wave and a subsequent exothermic reaction zone move together at a characteristic speed called the Chapman-Jouguet (CJ) detonation speed. It is an important aspect of a detonation that a hot, high-pressure, high-speed gas flow is induced behind the exothermic reaction zone (Ref 1, 2). Therefore, hot, high-pressure, high-speed gas jets are intermittently obtained when a series of pulsed detonations is cyclically generated in a tube, one end of which is closed and the other end is open. Such a technology is sometimes called the pulse detonation technology (PDT).

The PDT has been developed in the fields of aerospace propulsion and thermal spray, almost independently. In the field of aerospace propulsion, an internal combustion engine by means of the PDT is called a pulse detonation engine, which has been developed since the middle of the

T. Endo, R. Obayashi, T. Tajiri, K. Kimura, Y. Morohashi, and **T. Johzaki**, Department of Mechanical Systems Engineering, Hiroshima University, Higashi-Hiroshima, Japan; **K. Matsuoka**, Department of Aerospace Engineering, Nagoya University, Nagoya, Japan; and **T. Hanafusa** and **S. Mizunari**, Eastern Region Industrial Research Center, Hiroshima Prefectural Technology Research Institute, Fukuyama, Japan. Contact e-mail: takumaendo@hiroshima-u.ac.jp.

Nomenclature

a_{CJ}	Equilibrium sound speed of the burned gas in the Chapman-Jouguet state
a_g	Sound speed of the gas
C_D	Drag coefficient for a particle
c_{pg}	Specific heat of the gas at constant pressure
c_s	Specific heat of a particle
D_{CJ}	Chapman-Jouguet detonation speed
d_{DT}	Inner diameter of the detonation tube
d_s	Diameter of a particle
f	Fanning friction factor
$f_{n'}(\delta_{A1})$	Function of δ_{A1} whose form is determined by n'
H_g	Stagnation enthalpy of the burned gas
$H_{g,a}$	Enthalpy of the burned gas whose temperature is equal to that of the ambient atmosphere
k_B	Boltzmann constant
L_{DT}	Length of the detonation tube
L_s	Molar latent heat of fusion of the CoNiCrAlY alloy
$L_{s,i}$	Molar latent heat of fusion of pure metal i
Ma	Mach number of a particle
M_{CJ}	Propagation Mach number of the Chapman-Jouguet detonation
M_g	Mach number of the gas flow
m_i	Molecular mass of species i
m_s	Mass of a particle
n'	Parameter determined by γ_2 as $n' = (3 - \gamma_2)/[2(\gamma_2 - 1)]$
Nu	Nusselt number for a particle
p	Pressure of the gas
p_a	Pressure of the ambient atmosphere

p_{CJ}	Pressure of the burned gas in the Chapman-Jouguet state
$p_{plateau}$	Gas pressure on the closed end of the detonation tube when the detonation is propagating through the detonation tube
Pr	Prandtl number
$\dot{Q}$	Heat flow to a particle
Q_i	Time-averaged flow rate of gas i
R_a	Arithmetic mean roughness of a surface
Re	Reynolds number of a particle
Re_{DT}	Reynolds number of flow inside the detonation tube
R_u	Universal gas constant
t	Time whose origin ($t = 0$) is the ignition timing
t_1	Time at which the detonation is propagating at $x = -0.15$ m
t_2	Time at which the detonation arrives at the PDC exit ($x = 0$)
t_{cyc}	Period of cyclic PDC operation
$t_{exhaust}$	Time at which the gas pressure on the closed end of the detonation tube decreases to the initial pressure
T_g	Temperature of the gas
$T_{g,a}$	Temperature of the ambient atmosphere
$t_{plateau}$	Time at which the gas pressure on the closed end of the detonation tube begins to decrease from $p_{plateau}$
T_s	Temperature of a particle
u_g	Flow speed of the gas
$u_{g,x<0}$	Flow speed of fresh explosive gas inside the PDC
u_s	Speed of a particle
υ_{CJ}	Specific volume of the burned gas in the Chapman-Jouguet state
W_g	Average molar mass of the burned gas in the Chapman-Jouguet state
x	Coordinate along the central axis of the detonation tube, whose direction is from the closed end toward the exit and whose origin ($x = 0$) is at the exit
X_i	Mole fraction of species i
x_s	Position of a particle
Y	Mass fraction
Y_i	Mass fraction of metallic component i in the CoNiCrAlY alloy
α	Heat transfer coefficient for a particle
γ_1	Specific-heat ratio of fresh explosive gas
γ_2	Effective specific-heat ratio of the burned gas in the Chapman-Jouguet state
δ_{A1}	Dimensionless quantity determined by M_{CJ}, γ_1, and γ_2
Δt	Time step in model calculation
ε_{DT}	Surface roughness of the inner wall of the detonation tube
ε_i	Lennard-Jones potential well depth of species i
Φ_{ij}	Dimensionless quantity used for the evaluation of the viscosity of the gas mixture
λ_g	Thermal conductivity of the gas
μ_g	Viscosity of the gas
μ_{gs}	Viscosity of the gas evaluated at the particle temperature
μ_i	Viscosity of pure species i
ρ_g	Mass density of the gas
$\rho_{g,a}$	Mass density of the burned gas whose temperature and pressure are equal to those of ambient atmosphere
ρ_s	Mass density of the CoNiCrAlY alloy
$\rho_{s,i}$	Mass density of pure metal i
σ_i	Lennard-Jones collision diameter of species i
τ_{jet}	Duration of the exhaust jet from the detonation tube
$\Omega_{\mu i}$	Dimensionless quantity used for the evaluation of the viscosity of pure species i

Subscript

0	Gun exit

Abbreviations

CJ	Chapman-Jouguet
GAP	Inert gas purge
LIP	Liquid purge
PDC	Pulse detonation combustor
PDT	Pulse detonation technology
slm	Standard liter per minute
SOFC	Solid oxide fuel cell
TBC	Thermal barrier coating
YSZ	Yttria-stabilized zirconia

last century (Ref 3-8). In addition, in recent years, PDT-based gas-turbine engines operated on the ground have been under development (Ref 9, 10). Almost independently of such development in the field of propulsion and power, thermal spray technologies based on the PDT have been developed since the middle of the last century as well. The thermal spray technology based on the PDT, such as the detonation gun process, can spray coatings with high bond strengths and low porosity (Ref 11-17).

The PDT is a technology in which pulsed detonations are cyclically initiated by controlled spark ignitions in a combustor. Therefore, it is important that the residual hot burned gas of the previous cycle is purged by some means before refilling the combustor with fresh explosive gas for the next cycle. Otherwise, the supplied fuel and oxidizer uncontrollably start to burn as a result of the heat transfer from the residual hot burned gas of the previous cycle, and refilling the combustor fully with fresh explosive gas becomes impossible. This purge process is critically important for the stable high-frequency operation of a pulse detonation combustor (PDC), and often limits the operation frequency of a PDC.

Several years ago, a technology for high-frequency operation of a PDC, where all valves are kept open, was developed by the authors, and the PDC was successfully operated at up to 200 Hz (Ref 18). The principles of this operation technology are simple and as follows. The PDC is a tube, one end of which is closed and the other end is open, and three gas-feeding pipes for fuel gas, oxygen gas, and inert gas are connected to the closed end of the PDC. The supply pressures of the fuel and oxygen gases are set equally, but only the supply pressure of the inert gas is set

higher. After the ignition of the explosive gas by a spark plug and subsequent initiation of a detonation, the gas pressure inside the PDC becomes high and, thereby, the supply of all gases stops. After the detonation reaches the open end of the PDC, an exhausting rarefaction wave propagates from the open end toward the closed end. In addition, after the exhausting rarefaction wave reaches the closed end, the gas pressure around the exits of the gas-feeding pipes decreases. Because the supply pressure of the inert gas is set higher than those of the fuel and oxygen gases, only the inert gas is first supplied into the PDC. In addition, after the gas pressure around the exits of the gas-feeding pipes further decreases, the fuel and oxygen gases are supplied with some delay compared to the inert gas. As a result of this delayed supply of the fuel and oxygen gases, the residual hot burned gas of the previous cycle is purged by the earlier-supplied inert gas. In this mode, the operation of the PDC is controlled by the spark ignitions only. In this paper, this operation mode of a PDC is called the inert gas purge (GAP) mode. The operation of a PDC in the GAP mode is very stable and durable because the GAP-mode operation of a PDC is free of moving components, and a PDC was successfully operated in the GAP mode at 150 Hz for 15 min continuously by the authors (Ref 19). Although the operation of a PDC in the GAP mode is very stable and durable, pure fuel-oxygen combustion is impossible because the explosive gas is, in principle, diluted by the inert gas for the purge process. This indicates that the burning temperature in the GAP-mode operation of a PDC is lower compared to the case of pure fuel-oxygen detonation.

Recently, another high-frequency operation mode of a PDC, which is called the liquid-purge (LIP) mode, was developed by the authors (Ref 20). In the LIP-mode operation of a PDC, the residual hot burned gas of the previous cycle is purged by using the liquid-to-gas phase transition of injected liquid droplets. The principles of the LIP-mode operation of a PDC are as follows. The PDC is a tube, one end of which is closed and the other end is open, and two gas-feeding pipes for fuel and oxygen gases are connected to the closed end of the PDC. Furthermore, a liquid-droplet injector is installed at the closed end for injecting liquid droplets into the PDC for the purge process. The fuel and oxygen gases are supplied into the PDC in a valveless mode, similar to the GAP mode where all valves are kept open and the supply of the gases is controlled by the difference between the supply pressure of the gases and the gas pressure around the exits of the gas-feeding pipes. In the LIP mode, during the final stage of the gas supply, specifically just before the detonation initiation, liquid droplets are injected in the vicinity of the closed end. After the ignition of the explosive gas by a spark plug and subsequent initiation of detonation, the gas pressure inside the PDC increases, and thereby, the supply of all gases stops. In addition, at that time, the liquid-to-gas phase transition of the injected liquid droplets begins in the hot burned gas, in the vicinity of the closed end. The liquid-to-gas phase transition is endothermic and accompanied by a roughly thousand-fold volume expansion, and thereby, the hot burned gas is cooled and pushed toward the open end, namely purged. That is, the LIP-mode operation of a PDC is controlled by the spark ignitions and the synchronized liquid-droplet injection. A PDC was successfully operated in the LIP mode at up to 350 Hz (Ref 20). Although the liquid-droplet injector has to be actuated every cycle, pure fuel-oxygen combustion is possible in the LIP mode (Ref 20). This indicates that the burning temperature in the LIP-mode operation of a PDC is higher compared to the GAP mode.

These technologies for the high-frequency operation of a PDC developed by the authors, that is, the GAP and LIP modes, require inert gas or liquid, which is usually water, for the purge process. Therefore, these technologies are suitable for ground applications, rather than aerospace applications, and thermal spray seems their most suitable application field. So far, detonation guns of various types for thermal spray have already been developed (Ref 11, 12, 15, 21-34), and some of them are named, such as the D-Gun (Ref 11, 12, 24), ADK-1M (Ref 15), KORUND (Ref 21), Ob (Ref 17, 22), Perun P (Ref 25), and HFPD (Ref 26-34). All detonation guns except HFPD are rather large, typically 1-m long or more, and operate at low frequencies, typically several Hz. Only the HFPD detonation gun is rather small, 0.5-0.9 m long (Ref 26), and ordinarily operates at 45-75 Hz (Ref 27-34). The HFPD detonation gun is operated by the valveless-mode fuel-and-oxygen supply, where the hot burned gas backflows into the gas-feeding pipes and is rapidly cooled there, and the cooled burned gas is reintroduced into the PDC for utilization in the purge process (Ref 26). The PDCs developed by the authors experience the backflows of the burned gas into the gas-feeding pipes as well as the HFPD detonation gun. However, in the PDCs developed by the authors, it is not expected that the burned gas cooled in the gas-feeding pipes purges the hot burned gas of the previous cycle, but expected that the introduced inert gas or vapor of the introduced liquid droplets purges the hot burned gas of the previous cycle. Compared with the existing detonation guns for thermal spray, the PDC developed by the authors can be operated at higher frequencies and, therefore, has the possibility to be downsized without sacrificing spray rate. Accordingly, it is significant to experimentally investigate the ability of the developed high-frequency PDCs regarding thermal spray from the viewpoint of the application of high-frequency PDT.

This paper shows the results of the experimental investigations of the ability of the developed high-frequency PDCs to heat and accelerate solid particles by using CoNiCrAlY and yttria-stabilized zirconia (YSZ). These materials were chosen because CoNiCrAlY is often used for thermal barrier coatings (TBCs) (Ref 35) and YSZ is often used for TBCs (Ref 35) and solid oxide fuel cells (SOFCs) (Ref 36). In the following sections, first described are the experimental measurements of temperature and speed of in-flight CoNiCrAlY particles heated and accelerated by using high-frequency PDCs operated in the GAP and LIP modes. Next, the experimental results are compared with the results of simple model calculations, and the difference in the particle heating and

acceleration processes between the GAP and LIP modes is discussed. After that, experiments on the thermal spray of YSZ using a high-frequency PDC operated in the LIP mode are described. Finally, the main conclusions are summarized.

2. Experimental Arrangement

In the experiments, two types of PDCs were used, one operated in the GAP mode and the other in the LIP mode. The PDCs used in the experiments are shown in Fig. 1 and 2. Both PDCs were made of stainless steel, 10 mm in inner diameter, 350 mm in length, and were water-cooled. Automotive spark plugs (NGK, R847-11) were used for ignition. A 1.5-mm-inner-diameter powder supply nozzle was installed in each PDC at 150 mm from the PDC exit. Although detonations were intermittently initiated in the PDC, the powder was continuously supplied to the PDC using a commercially available powder feeder (GTV, PF 2/1) together with a carrier gas (argon) whose flow rate was 20 standard liter per minute (slm) and supply pressure was 1.09 MPa. In this paper, pressure is shown in absolute pressure, and the gas flow rate is shown in slm, which is the volume flow rate converted to standard conditions: 20 °C and 1 atm. The fuel was ethylene, and the oxidizer was oxygen. In all experiments, gases were supplied to the PDCs in the valveless mode, and their time-averaged flow rates were controlled using commercially available mass flow controllers.

In the GAP-mode operation, argon was used as the purging gas, which was supplied to the PDC inclined 45° from the tube axis toward the closed end, as shown in Fig. 1. Ethylene and oxygen were supplied to the PDC in opposing directions for quick mixing. Two spark plugs were installed at 57 and 77 mm from the closed end.

In the LIP-mode operation, a liquid injector, which was a fuel injector (MITSUBISHI, 1465A010) used in an automobile gasoline direct injection engine, was installed at the closed end, as shown in Fig. 2. By using the liquid injector, water droplets were injected at a supply pressure of 7.1 MPa into the PDC, where the Sauter mean diameter of the water droplets was 24.4 μm and the spray cone angle was 35° (half angle). Taking into account the spray cone angle of the water droplets, the gas-feeding pipes for the ethylene and oxygen were installed in the PDC at an angle of 35° from the tube axis, as shown in Fig. 2. A spark plug was installed in the PDC 50 mm from the closed end.

The powders used in the experiments were CoNiCrAlY (Oerlikon Metco, Amdry 9951) (Ref 37), with a mass ratio of Co:Ni:Cr:Al:Y = 5:4:2.5:1:0.05 and a melting point of about 1340 °C (Ref 38), and ZrO_2-8 wt.% Y_2O_3 (Oerlikon Metco, Metco 204NS) (Ref 39), with a melting point of about 2800 °C. Figure 3 and 4 show a photograph and particle-size distribution of the CoNiCrAlY powder and the ZrO_2-8 wt.% Y_2O_3 (YSZ) powder, respectively. Here, d_s and $Y(d_s)$ denote the particle diameter and mass fraction, respectively. The number of particles of a specified diameter d_s is proportional to $Y(d_s)/d_s^3$. For the particle-size distribution shown in Fig. 3(b), the number fractions of CoNiCrAlY particles are 0.37 for d_s = 5-10 μm, 0.49 for d_s = 10-20 μm, 0.13 for d_s = 20-38 μm, and 0.0015 for d_s = 38-45 μm, where the medium value of each diameter bin in Fig. 3(b) was used as d_s in the calculations of $Y(d_s)/d_s^3$. In addition, the average diameter weighted by the mass fraction was 24 μm, although the average diameter weighted by the number fraction was 14 μm. For the particle-size distribution shown in Fig. 4(b), the number fractions of YSZ particles are 0.71 for d_s = 11-24 μm, 0.26 for d_s = 24-54 μm, 0.034 for d_s = 54-99.5 μm, and 0.0027 for d_s = 99.5-125 μm. In addition, the average diameter weighted by the mass fraction was 59 μm, although the average diameter weighted by the number fraction was 25 μm.

For the measurements of the temperature and speed of the in-flight particles, SprayWatch 2i (Oseir Ltd., Finland) was used, which was based on a single CCD camera with a field of view about 21 mm in the horizontal direction and about 28 mm in the vertical direction and a depth of about 6 mm. The temperature of the particles was measured by

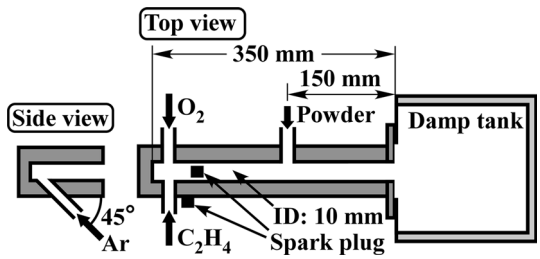

Fig. 1 Pulse detonation combustor (PDC) for the inert gas purge (GAP) mode operation

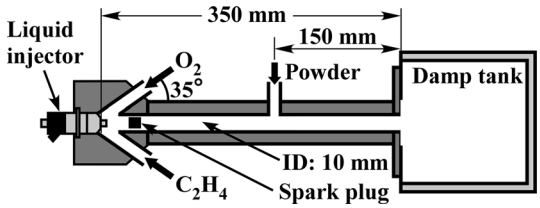

Fig. 2 PDC for the liquid-purge (LIP) mode operation

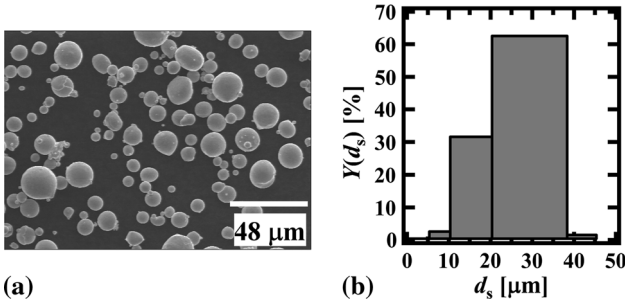

Fig. 3 Photograph (a) and particle-size distribution (b) of the CoNiCrAlY powder

two-color pyrometry at 700 and 850 nm, where the measurement time duration was set to 0.2 ms. The particle speeds were measured from the length of the particle traces during the known exposure time, which was set to 0.5 μs. Although the heating and acceleration processes of a particle depend on its size, any information about the sizes of the diagnosed particles cannot be obtained by this diagnostic equipment. In this sense, the temperature and speed measured by SprayWatch 2i mean the typical temperature and speed of the in-flight particles.

3. Heating and Acceleration of CoNiCrAlY Particles in GAP and LIP Modes

3.1 Experiments

The operation conditions of the PDCs in the GAP and LIP modes are summarized in Table 1. The parameters of the CJ detonations were calculated using the chemical equilibrium calculation software STANJAN (Ref 40) for an initial temperature of 300 K and an initial pressure of 1 atm. Both PDCs were operated at 150 Hz for 20 s. The supply rate of the CoNiCrAlY powder was 20 g/min. The center of the field of view of SprayWatch 2i was set 100 mm from the PDC exit on the elongation of the PDC axis, and the start time of the measurement was varied every 0.2 ms from the ignition timing by which the time origin $t = 0$ was defined. The temperature and speed of the in-flight particles were measured without a substrate to be sprayed.

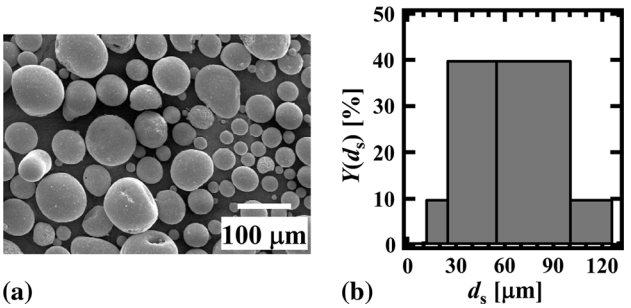

Fig. 4 Photograph (a) and particle-size distribution (b) of the yttria-stabilized zirconia (YSZ) powder

The measured temperature and speed of the CoNiCrAlY particles are shown in Fig. 5, where T_s and u_s denote the temperature and speed of the particles, respectively. The vertical error bars show the standard deviations of the data, and the horizontal error bars correspond to the time duration of the temperature measurement. The time regions in which data are not plotted correspond to the time regions in which the self-emission of the particles was too weak to be observed. The time duration in which the experimental data were obtained was about 1.2 ms per cycle for both of the GAP and LIP modes. This value can be explained from the analysis of the wave dynamics in a detonation tube. The duration of the exhaust jet from a detonation tube τ_{jet} corresponds to the difference between the time when a detonation reaches the exit of the detonation tube and the time when the gas pressure on the closed end of the detonation tube returns to the initial pressure. According to Ref 7, τ_{jet} is given by the following formula.

$$\tau_{jet} = \left\{ 2\frac{\gamma_1 M_{CJ}^2}{\gamma_1 M_{CJ}^2 + \gamma_2}\left[f_{n'}(\delta_{A1}) - 1\right] + 2\left(\frac{\gamma_1 M_{CJ}^2 + \gamma_2}{\gamma_1 M_{CJ}^2 + 1}\frac{\gamma_2 + 1}{2\gamma_2}\right)^{-\frac{\gamma_2+1}{2(\gamma_2-1)}} - 1 \right\} \frac{L_{DT}}{D_{CJ}}$$

$$\left[\delta_{A1} = \frac{\gamma_1 M_{CJ}^2 + \gamma_2}{2\gamma_2}\left(\frac{\gamma_1 M_{CJ}^2 + \gamma_2}{\gamma_1 M_{CJ}^2 + 1}\frac{\gamma_2 + 1}{2\gamma_2}\right)^{\frac{\gamma_2+1}{\gamma_2-1}}\right] \quad \text{(Eq 1)}$$

In the above formula, L_{DT} denotes the detonation tube length, D_{CJ} denotes the CJ detonation speed, M_{CJ} denotes the propagation Mach number of the CJ detonation, γ_1 denotes the specific-heat ratio of the fresh explosive gas, γ_2 denotes the effective specific-heat ratio of the burned gas in the CJ state, and $f_{n'}(\delta_{A1})$ is a function of δ_{A1} whose form is determined by $n' = (3 - \gamma_2)/[2(\gamma_2 - 1)]$ and given in Ref 7. Calculating τ_{jet} for the conditions of the present experiments, τ_{jet} is approximately 1.3 ms for both the GAP and LIP modes, which agrees well with the above value (1.2 ms).

As shown in Fig. 5(a), the highest particle temperature observed in the LIP-mode operation was higher than that in the GAP-mode operation by about 1000 K. On the other hand, the CJ temperature for the LIP-mode operation was higher than that for the GAP-mode operation by

Table 1 Operation conditions of PDCs for experiments on CoNiCrAlY particles

Operation mode	GAP	LIP
Supply pressure of C_2H_4 and O_2, MPa	0.60	0.50
Supply pressure of Ar, MPa	1.09	…
Supply rate of C_2H_4, slm	88	106
Supply rate of O_2, slm	240	300
Supply rate of Ar, slm	600	…
Composition of explosive gas	$1.1C_2H_4 + 3O_2 + 6.4Ar$	$1.1C_2H_4 + 3O_2$
Temperature at CJ surface, K	3597	3968
Pressure at CJ surface, MPa	2.512	3.496
Gas speed at CJ surface relative to the unburned gas, m/s	857	1114
Mass of injected water per cycle, mg	…	25

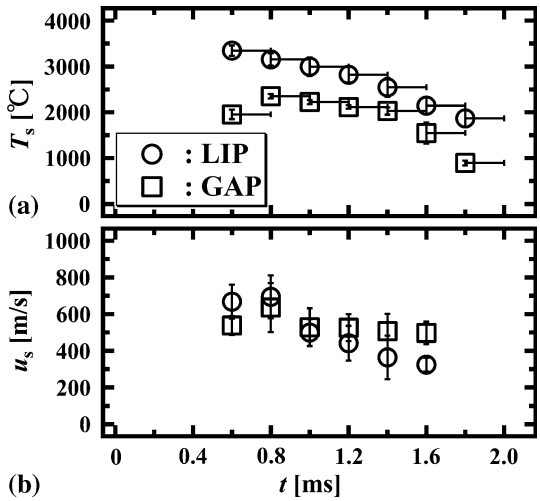

Fig. 5 Measured temperature (a) and speed (b) of the in-flight CoNiCrAlY particles

about 370 K, as shown in Table 1. The difference in the CJ temperature between the two different operation modes seems to have the largest influence on the difference in the particle temperature between the two different operation modes measured at the time when the self-emission of the particles begins to be observable, namely at $t = 0.6$ ms. However, the particle temperature measured at that time for the LIP-mode operation was higher than that for the GAP-mode operation by about 1400 K. That is, the experimental results showed that the difference in the particle temperature measured at $t = 0.6$ ms between the two different operation modes was much larger than the difference in the CJ temperature between the two different operation modes. In contrast, regarding the speed, the speed of the gas flow induced by the CJ detonation for the LIP-mode operation was higher than that for the GAP-mode operation by about 260 m/s, as shown in Table 1. The difference in the speed of the detonation-induced gas flow between the two different operation modes seems to have the largest influence on the difference in the particle speed between the two different operation modes measured at $t = 0.6$ ms. However, the particle speed measured at that time for the LIP-mode operation was higher than that for the GAP-mode operation only by about 130 m/s. Further, the highest particle speed measured for the LIP-mode operation was higher than that for the GAP-mode operation only by about 50 m/s. That is, on the contrary to the case of the particle temperature, the experimental results showed that the difference in the particle speed measured at $t = 0.6$ ms between the two different operation modes was much smaller than the difference in the speed of the detonation-induced gas flow between the two different operation modes. Summarizing the above results, the differences in the measured particle temperature and speed between the two different operation modes were qualitatively as expected, but quantitatively not. In the following section, the experimental results are quantitatively discussed by comparing them with the results of simple model calculations.

3.2 Model Calculations

In section 3.2, described are the detailed methods for the calculations for the particle temperature and speed measured at the time when the self-emission of the particles begins to be observable, namely at $t = 0.6$ ms. In the model calculations, the x-axis is set as the central axis of the PDC, whose direction is from the closed end toward the exit and whose origin ($x = 0$) is at the exit, and the temperature and speed of a particle only on the x-axis are calculated. The boundary conditions for the particle temperature and speed are $T_s = 300$ K and $u_s = 0$ at $x = -150$ mm, corresponding to the location of the powder feeding nozzle, as shown in Fig. 1 and 2. The initial conditions for the thermodynamic state of all gaseous media are $p = 1$ atm and $T_g = 300$ K, where p and T_g denote the pressure and temperature of the gaseous media, respectively. Because the objective of the present model calculations is to calculate the particle temperature and speed measured at the time when the self-emission of the particles begins to be observable, the following situation is assumed. Initially, fresh explosive gas flows through the PDC, namely a straight tube, toward the exit, and a spherical particle of a specified diameter is accelerated by the flow of fresh explosive gas. After the ignition, a CJ detonation propagates toward the PDC exit. At a certain instant, both the particle and the detonation arrive simultaneously at the PDC exit. After that time, the particle is heated and accelerated by the jet of the burned gas outside the PDC. The assumed situation is explained some more. Let us consider particles of a specified diameter. In the present work, solid particles were continuously supplied to the PDC although detonations were intermittently initiated. Therefore, before ignition, particles of a specified diameter existed in the fresh explosive gas flow inside the PDC everywhere between the powder feeding nozzle and the PDC exit and also outside the PDC. Accordingly, a group of such particles necessarily encountered a detonation at the PDC exit. Indeed, another group of such particles supplied earlier to the PDC encountered a hot burned gas jet outside the PDC and reached the field of view of SprayWatch 2i earlier than the particles encountering a detonation at the PDC exit. However, for simplicity, it was assumed that the particles encountering a detonation at the PDC exit contributed the experimental data measured at the time when the self-emission of the particles began to be observable.

In the model calculations, the position x_s, speed $u_s = \mathrm{d}x_s/\mathrm{d}t$, and temperature T_s of the spherical particle of a specified diameter are calculated as a function of time t using the following formulae:

$$x_s(t + \Delta t) = x_s(t) + u_s(t)\Delta t \qquad \text{(Eq 2)}$$

$$u_s(t + \Delta t) = u_s(t) + C_D \frac{1}{2}\rho_g \frac{(u_g - u_s)^3}{|u_g - u_s|}\frac{\pi d_s^2}{4}\frac{1}{m_s}\Delta t \qquad \text{(Eq 3)}$$

$$T_s(t+\Delta t) = T_s(t) + \alpha \frac{(T_g - T_s)\pi d_s^2}{m_s c_s}\Delta t \quad \text{(Eq 4)}$$

In the above formulae, Δt denotes a small time step set to 1 μs in the present calculations, C_D denotes the drag coefficient for the particle, ρ_g denotes the mass density of the gas, u_g denotes the flow speed of the gas, m_s denotes the particle mass, α denotes the heat transfer coefficient for the particle, and c_s denotes the specific heat of the particle. The nonuniformity of the temperature in the particle is ignored. When the particle temperature is equal to the melting point (1340 °C), the heat flow to the particle $\dot{Q}$ is evaluated by the formula $\dot{Q} = \alpha(T_g - T_s)\pi d_s^2$, and the particle temperature is equal to the melting point until the fusion of the particle finishes. In addition, the influence of the heating and acceleration of the particles on the thermodynamic and gasdynamic states of the gas flow was ignored. This was because the mass flow rate of the supplied gas was 1418 g/min in the GAP-mode operation and 523 g/min in the LIP-mode operation, which were much larger than the mass flow rate of the CoNiCrAlY powder, which was 20 g/min. More detailed calculation methods are described below.

3.2.1 Calculation Methods for the Drag Coefficient C_D and Heat Transfer Coefficient α. The drag coefficient for the particle is evaluated by the following formula (Ref 41, 42).

$$C_D = \frac{24}{Re}\left(1 + 0.1806Re^{0.6459} + \frac{Re}{24}\frac{0.4251}{1+\frac{6880.95}{Re}}\right) \times \frac{1+\exp\left(-\frac{0.427}{Ma^{4.63}} - \frac{3}{Re^{0.88}}\right)}{1+\frac{Ma}{Re}\left[3.82 + 1.28\exp\left(-1.25\frac{Re}{Ma}\right)\right]} \quad \text{(Eq 5)}$$

In the above formula, Re and Ma denote the Reynolds and Mach numbers of the particle, respectively, and are defined by

$$Re = \frac{\rho_g |u_g - u_s| d_s}{\mu_g}, \quad \text{(Eq 6)}$$

$$Ma = \frac{|u_g - u_s|}{a_g}, \quad \text{(Eq 7)}$$

where μ_g and a_g denote the viscosity and sound speed of the gas, respectively.

The heat transfer coefficient for the particle is evaluated by the following formula (Ref 42-45).

$$\alpha = Nu\frac{\lambda_g}{d_s} \times \left\{ Nu = \frac{2 + \left(0.4Re^{\frac{1}{2}} + 0.06Re^{\frac{2}{3}}\right)Pr^{0.4}\left(\mu_g/\mu_{gs}\right)^{\frac{1}{4}}}{1 + 3.42\frac{Ma}{RePr}\left[2 + \left(0.4Re^{\frac{1}{2}} + 0.06Re^{\frac{2}{3}}\right)Pr^{0.4}\left(\mu_g/\mu_{gs}\right)^{\frac{1}{4}}\right]} \right\} \quad \text{(Eq 8)}$$

In the above formula, Nu denotes the Nusselt number for the particle, λ_g denotes the thermal conductivity of the gas, μ_{gs} denotes the viscosity of the gas evaluated at the particle temperature, and Pr denotes the Prandtl number defined by

$$Pr = \frac{c_{pg}\mu_g}{\lambda_g} \quad \text{(Eq 9)}$$

where c_{pg} denotes the specific heat of the gas at constant pressure.

3.2.2 Calculation Methods for the Thermodynamic and Transport Parameters of Gas. The fresh explosive gas and the burned gas are treated as different kinds of calorically perfect gases, where a calorically perfect gas indicates an ideal gas with constant specific heats. The chemical composition of the burned gas is simplified so that it is the same as that of the CJ state computed using the chemical equilibrium calculation software STANJAN (Ref 40). The effective specific-heat ratio of the burned gas is evaluated by

$$\gamma_2 = \frac{a_{CJ}^2}{p_{CJ}\upsilon_{CJ}}, \quad \text{(Eq 10)}$$

where a_{CJ}, p_{CJ}, and υ_{CJ} denote the equilibrium sound speed, pressure, and specific volume of the burned gas in the CJ state, respectively. The specific heat of the burned gas at constant pressure is evaluated by

$$c_{pg} = \frac{\gamma_2}{\gamma_2 - 1}\frac{R_u}{W_g}, \quad \text{(Eq 11)}$$

where R_u denotes the universal gas constant and W_g denotes the average molar mass of the burned gas in the CJ state.

The viscosity of the gas is evaluated by the following formula (Ref 46).

$$\mu_g = \sum_i \frac{X_i\mu_i}{\sum_j X_j\Phi_{ij}} \quad \text{(Eq 12)}$$

In the above formula, X_i denotes the mole fraction of chemical species i and the quantities μ_i and Φ_{ij} are given by

$$\mu_i = \frac{5}{16}\frac{\sqrt{\pi m_i k_B T_g}}{\pi\sigma_i^2\Omega_{\mu i}}, \quad \text{(Eq 13)}$$

$$\Phi_{ij} = \frac{1}{\sqrt{8}}\left(1 + \frac{m_i}{m_j}\right)^{-\frac{1}{2}}\left[1 + \left(\frac{\mu_i}{\mu_j}\right)^{\frac{1}{2}}\left(\frac{m_j}{m_i}\right)^{\frac{1}{4}}\right]^2, \quad \text{(Eq 14)}$$

where m_i denotes the molecular mass of chemical species i, k_B denotes the Boltzmann constant, σ_i denotes the Lennard-Jones collision diameter of chemical species i, and the quantity $\Omega_{\mu i}$ is given by the following formula (Ref 47).

$$\Omega_{\mu i} = \frac{1.155}{\left(k_B T_g/\varepsilon_i\right)^{0.1462}} + \frac{0.3945}{\exp\left(0.6672k_B T_g/\varepsilon_i\right)} + \frac{2.05}{\exp\left(2.168k_B T_g/\varepsilon_i\right)} \quad \text{(Eq 15)}$$

In the above formula, ε_i denotes the Lennard-Jones potential well depth of chemical species i. The values of the Lennard-Jones collision diameter σ_i and the Lennard-Jones potential well depth ε_i are given in

Table 4.3 of Ref 47. Taking into account the correction for the polar molecule H_2O, the quantity $\Omega_{\mu H_2O}$ is given by the following formula (Ref 48).

$$\Omega_{\mu H_2O} = \frac{1.155}{(k_B T_g/\varepsilon_i)^{0.1462}} + \frac{0.3945}{\exp(0.6672 k_B T_g/\varepsilon_i)} + \frac{2.05}{\exp(2.168 k_B T_g/\varepsilon_i)} + \frac{0.2 \times 1.217^2}{k_B T_g/\varepsilon_i} \quad \text{(Eq 15a)}$$

The thermal conductivity of the gas is simply given by the following modified Eucken correlation (Ref 49) from the evaluated viscosity of the gas μ_g.

$$\lambda_g = R_u \left(\frac{1.32}{\gamma_2 - 1} + 1.77 \right) \frac{\mu_g}{W_g} \quad \text{(Eq 16)}$$

3.2.3 Calculation Methods for the Thermodynamic Parameters of the CoNiCrAlY Particles. In order to calculate the heating and acceleration processes of a CoNiCrAlY particle, the values of mass density ρ_s, specific heat c_s, and molar latent heat of fusion L_s of the CoNiCrAlY alloy are needed. The mass density of the CoNiCrAlY alloy is evaluated by

$$\rho_s = \frac{1}{\sum_i Y_i/\rho_{s,i}}, \quad \text{(Eq 17)}$$

where Y_i denotes the mass fraction of metallic component i in the CoNiCrAlY alloy and $\rho_{s,i}$ denotes the mass density of pure metal i. The molar latent heat of fusion of the CoNiCrAlY alloy is evaluated by

$$L_s = \sum_i X_i L_{s,i}, \quad \text{(Eq 18)}$$

where X_i denotes the mole fraction of metallic component i in the CoNiCrAlY alloy and $L_{s,i}$ denotes the molar latent heat of fusion of pure metal i. The specific heat of the CoNiCrAlY alloy is evaluated by the following formula, referring to the data given in Ref 50.

$$c_s[\mathrm{J/(kg\ K)}] = \begin{cases} 350 + 0.268 \times T_s[^\circ\mathrm{C}] & \text{for } T_s < 1340 \\ 708 & \text{for } 1340 \le T_s \end{cases} \quad \text{(Eq 19)}$$

3.2.4 Calculation Methods for the Gas Flow State Inside the PDC. The gas flow state of the fresh explosive gas inside the PDC is evaluated as follows. The time-averaged flow rates of ethylene $Q_{C_2H_4}$, oxygen Q_{O_2}, and argon Q_{Ar} supplied into the PDC are known. However, these gases are supplied into the PDC in the valveless mode; therefore, their instantaneous flow rates are determined by the relation between their supply pressures and the instantaneous gas pressure in the vicinity of the exits of the gas-feeding pipes. The time history of the gas pressure in the vicinity of the exits of the gas-feeding pipes is simply approximated by the analytical solution given in Ref 7 on the time history of the gas pressure on the closed end of a detonation tube, one end of which is closed and the other end is open. According to Ref 7, on the assumption that a CJ detonation begins to propagate in an explosive gas at rest from the closed end toward the open end at time $t = 0$, the pressure on the closed end is constant at $p_{plateau}$ until the time $t_{plateau}$. After that time, the pressure gradually decreases to the initial pressure at time $t_{exhaust}$. Assuming that the initial pressure and temperature of the fresh explosive gas are respectively 1 atm and 300 K, it is evaluated that $t_{plateau} = 0.58$ ms, $p_{plateau} = 0.92$ MPa, and $t_{exhaust} = 1.44$ ms for the GAP-mode operation where $\gamma_1 = 1.4685$, $\gamma_2 = 1.1697$, $D_{CJ} = 1901.3$ m/s, and $M_{CJ} = 5.9959$. In addition, $t_{plateau} = 0.46$ ms, $p_{plateau} = 1.28$ MPa, and $t_{exhaust} = 1.43$ ms for the LIP-mode operation where $\gamma_1 = 1.3255$, $\gamma_2 = 1.1411$, $D_{CJ} = 2423.8$ m/s, and $M_{CJ} = 7.4145$. In the present experiments, the supply pressure of argon was 1.09 MPa, and that of ethylene and oxygen was 0.60 MPa for the GAP-mode operation and 0.50 MPa for the LIP-mode operation, as shown in Table 1. Therefore, the effective supply duration of argon in a cycle is simplified from $t_{plateau}$ to t_{cyc} (1/150 s), and that of ethylene and oxygen in a cycle is simplified from $t_{exhaust}$ to t_{cyc}, where t_{cyc} is the period of the cyclic operation at 150 Hz. By using the above simplification, the flow speed of the fresh explosive gas inside the PDC $u_{g,x<0}$ is evaluated by the following formula:

$$u_{g,\,x<0} = \frac{4}{\pi d_{DT}^2} \left[\frac{Q_{Ar} t_{cyc}}{t_{cyc} - t_{plateau}} + \frac{(Q_{C_2H_4} + Q_{O_2}) t_{cyc}}{t_{cyc} - t_{exhaust}} \right] \quad \text{(Eq 20)}$$

In the above formula, d_{DT} denotes the inner diameter of the PDC. By using the above formula, it is evaluated that $u_{g,x<0} = 228$ m/s for the GAP-mode operation and $u_{g,x<0} = 110$ m/s for the LIP-mode operation. In summary, the gas flow state of the fresh explosive gas in the region of $x < 0$ is given by the uniform steady flow of $p = 1$ atm and $T_g = 300$ K with a flow speed of $u_{g,x<0}$.

Here, the assumption of $p = 1$ atm stated above is examined. The Fanning friction factor f for a steady flow inside a straight cylindrical tube is defined by

$$f = \frac{d_{DT}}{2\rho_g u_g^2} \frac{\Delta p}{\Delta x}, \quad \text{(Eq 21)}$$

where $\Delta p/\Delta x$ denotes the pressure drop per unit length. According to Ref 51, the Fanning friction factor is given by the following formula:

$$f = \left[-4.0 \log_{10} \left(\frac{\varepsilon_{DT}/d_{DT}}{3.7065} - \frac{5.0272}{Re_{DT}} \log_{10} \left\{ \frac{\varepsilon_{DT}/d_{DT}}{3.827} - \frac{4.567}{Re_{DT}} \log_{10} \left[\left(\frac{\varepsilon_{DT}/d_{DT}}{7.7918} \right)^{0.9924} + \left(\frac{5.3326}{208.815 + Re_{DT}} \right)^{0.9345} \right] \right\} \right) \right]^{-2}$$
$$(3 \times 10^3 \le Re_{DT} \le 1.5 \times 10^8, \quad 0 \le \varepsilon_{DT}/d_{DT} \le 5 \times 10^{-2}) \quad \text{(Eq 22)}$$

In the above formula, ε_{DT} denotes the surface roughness of the inner wall of the tube and Re_{DT} denotes the Reynolds number of the flow inside the tube defined by

$$Re_{DT} = \frac{\rho_g u_{g,\,x<0} d_{DT}}{\mu_g}. \qquad \text{(Eq 23)}$$

Based on the assumption $\varepsilon_{DT}/d_{DT} \approx 10^{-3}$, it is evaluated that $f \approx 0.0053$ for the GAP-mode operation, where $\mu_g = 2.07 \times 10^{-5}$ Pa s and $Re_{DT} = 1.63 \times 10^5$, and $f \approx 0.0057$ for the LIP-mode operation, where $\mu_g = 1.70 \times 10^{-5}$ Pa s and $Re_{DT} = 8.10 \times 10^4$. Although the above values of the Reynolds number imply that the flows inside the PDC are intrinsically turbulent without powder injection, the intrinsic turbulence of the flows is ignored in the present model calculations for simplicity. From the evaluated values of the Fanning friction factor, the pressure drop for $\Delta x = 150$ mm, which is the distance between the powder-injection nozzle and the PDC exit, is estimated to be 0.12 atm for the GAP-mode operation and 0.025 atm for the LIP-mode operation. From these estimated values of the pressure drop, it is considered that the assumption of $p = 1$ atm does not contribute significant errors.

3.2.5 Calculation Methods for the Gas Flow State Outside the PDC. A particle that is accelerated by the flow of fresh explosive gas until it arrives at the PDC exit is heated and accelerated by the jet of the burned gas outside the PDC. In the present model calculations, the gas flow state at the PDC exit, which is denoted by subscript 0, is simplified to be equal to that at the CJ surface of the detonation because the objective of the present model calculations is to calculate the particle temperature and speed measured at the time when the self-emission of the particles begins to be observable. That is, the parameters at the PDC exit are set so that $p_0 = 2.512$ MPa, $T_{g,0} = 3597$ K, $\rho_{g,0} = 2.694$ kg/m^3, and $u_{g,0} = D_{CJ} - a_{CJ} + u_{g,x<0} = 1085$ m/s for the GAP-mode operation, and $p_0 = 3.496$ MPa, $T_{g,0} = 3968$ K, $\rho_{g,0} = 2.326$ kg/m^3, and $u_{g,0} = 1224$ m/s for the LIP-mode operation, where $D_{CJ} - a_{CJ}$ denotes the gas speed at the CJ surface of the detonation relative to the unburned gas. Furthermore, the Mach number of the burned gas jet at the PDC exit is given as $M_{g,0} = u_{g,0}/a_{CJ} = 1.0$ for the GAP-mode operation and $M_{g,0} = u_{g,0}/a_{CJ} = 0.93$ for the LIP-mode operation.

According to Ref 52 and 53, the flow speed and temperature of the burned gas jet on the x-axis outside the PDC are given by the following formulae, which were developed for steady jets.

$$\frac{u_g(x)}{u_{g,0}} = \begin{cases} 1 & \text{for } x \le L_c \\ 1 - \exp\left[-1\Big/\left(\kappa \frac{2x}{d_{DT}} \sqrt{\frac{\rho_{g,a}}{\rho_{g,0}}} - 0.70\right)\right] & \text{for } x > L_c \end{cases}$$
$$\left[\kappa = 0.08\left(1 - 0.16 M_{g,0}\right)\left(\rho_{g,a}/\rho_{g,0}\right)^{-0.22}, L_c = \frac{0.70 d_{DT}}{2\kappa\sqrt{\rho_{g,a}/\rho_{g,0}}}\right] \qquad \text{(Eq 24)}$$

$$\frac{H_g(x) - H_{g,a}}{H_{g,0} - H_{g,a}} = \begin{cases} 1 & \text{for } x \le \frac{0.70 d_{DT}}{0.204\sqrt{\frac{\rho_{g,a}}{\rho_{g,0}}}} \\ 1 - \exp\left[-1\Big/\left(0.102 \frac{2x}{d_{DT}} \sqrt{\frac{\rho_{g,a}}{\rho_{g,0}}} - 0.70\right)\right] & \text{for } x > \frac{0.70 d_{DT}}{0.204\sqrt{\frac{\rho_{g,a}}{\rho_{g,0}}}} \end{cases} \qquad \text{(Eq 25)}$$

In the above formulae, $\rho_{g,a}$ denotes the mass density of the burned gas whose temperature and pressure are equal to those of the ambient atmosphere, namely 300 K and 1 atm, and $H_g(x) = c_{pg} T_g(x) + \frac{1}{2}\left[u_g(x)\right]^2$, $H_{g,0} = c_{pg} T_{g,0} + \frac{1}{2} u_{g,0}^2$, and $H_{g,a} = c_{pg} T_{g,a}$, where $T_{g,a}$ denotes the temperature of the ambient atmosphere, namely 300 K. In the present calculations, $\rho_{g,a} = 1.302$ kg/m^3 for the GAP-mode operation and $\rho_{g,a} = 0.8919$ kg/m^3 for the LIP-mode operation. Regarding the burned gas pressure on the x-axis outside the PDC, the linear distribution given by the following formula is assumed because more appropriate empirical formulae or assumptions cannot be found by the authors.

$$p(x) = \begin{cases} p_0 - (p_0 - p_a)\frac{x}{L_c} & \text{for } x \le L_c \\ p_a & \text{for } x > L_c \end{cases} \qquad \text{(Eq 26)}$$

In the above formula, p_a denotes the pressure of the ambient atmosphere, namely 1 atm. Furthermore, the mass density of the burned gas on the x-axis outside the PDC is given by the following formula.

$$\rho_g(x) = \frac{p(x)}{p_0}\frac{T_{g,0}}{T_g(x)}\rho_{g,0} \qquad \text{(Eq 27)}$$

3.2.6 Determination of Representative Particle Diameters. In the experiments, the particle temperature and speed were measured by observing the self-emission from the CoNiCrAlY particles whose particle-size distribution is shown in Fig. 3(b). The observability of the particles with a specified diameter must be proportional to the product of the number of such particles and the cross-sectional area of such a particle, where this product is called the total cross-sectional area of the particles with a specified diameter hereafter. For the particle-size distribution of the mass fraction $Y(d_s)$, shown in Fig. 3(b), the number of particles with diameter d_s is proportional to $Y(d_s)/d_s^3$ and the cross-sectional area of such a particle is proportional to d_s^2; therefore, the total cross-sectional area of particles with diameter d_s is proportional to $Y(d_s)/d_s$. For the particle-size distribution of the mass fraction $Y(d_s)$, shown in Fig. 3(b), the normalized distribution of $Y(d_s)/d_s$ was calculated, where the medium value of each diameter bin in Fig. 3(b) was used as the denominator. The calculated normalized distribution of $Y(d_s)/d_s$ is

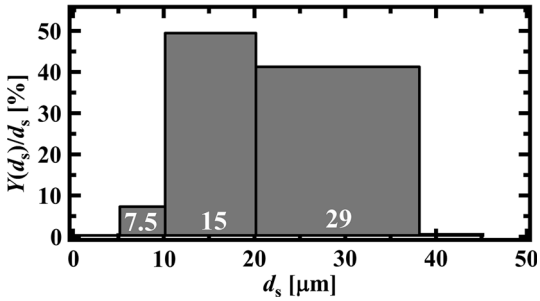

Fig. 6 Size distribution of the CoNiCrAlY particles for the total cross-sectional area of the particles with a specified diameter

shown in Fig. 6, in which the values of the representative diameter used in the calculations are also shown. As shown in Fig. 6, the particles whose diameters were in the range 10-38 μm must have dominant contributions to the present measurement. Accordingly, the model calculations were conducted for particles with diameters of 7.5, 15, 20, and 29 μm, where 15 and 29 μm are the representative diameters of particles having dominant contributions to the present measurement, 7.5 μm is for comparison, and 20 μm is the most typical diameter of particles having dominant contributions to the present measurement.

3.2.7 Determination of the Time Axis in the Model Calculations. The time axis in the model calculations should be comparable with the experiments and is determined as follows. First, preliminary experiments were conducted in which a pressure transducer was installed on the side wall of the PDC at a distance of $\Delta x = 150$ mm from the PDC exit, instead of the powder feeding nozzle, and the timing of the passage of a detonation t_1 was measured where the ignition timing was $t = 0$. By using the measured value of t_1, the timing t_2 at which the detonation arrived at the PDC exit was evaluated by the formula $t_2 = t_1 + \Delta x/(u_{g,x<0} + D_{CJ})$. The evaluated values of t_2 are $t_2 = 0.39$ ms for the GAP-mode operation and $t_2 = 0.28$ ms for the LIP-mode operation. In addition, the time axis in the model calculations is determined so that a particle accelerated by the flow of fresh explosive gas inside the PDC arrives at the PDC exit at t_2 evaluated above. This means that larger particles are considered to be supplied to the PDC through the powder feeding nozzle earlier than smaller particles.

3.3 Comparison Between Experiments and Model Calculations

Figure 7 shows the calculation results for the GAP-mode operation (the histories of the calculated particle temperature and speed as functions of the particle position) together with the corresponding experimental results (the particle temperature and speed measured at $t = 0.6$ ms and $x = 0.1$ m). Experimentally, at $x = 0.1$ m, the self-emission from the particles could not be observed at $t = 0.4$ ms, and the self-emission from the particles began to be observable from $t = 0.6$ ms. In the model calculations, the particles did not reach $x = 0.1$ m at $t = 0.4$ ms, but particles with diameters of 15, 20, and 29 μm, which must have dominant contributions to the measurement by SprayWatch 2i, reached the observation region at $t = 0.6$ ms taking into account the field of view of about 21 mm in the horizontal direction. In addition, the calculated temperature and speed of the particles with diameters of 15, 20, and 29 μm were close to the experimental results. Figure 8 shows a similar comparison between the model calculations and experiments for the LIP-mode operation. Further, for the LIP-mode operation, the experimental fact that the self-emission from the particles began to be observable from $t = 0.6$ ms was reproduced by the model calculations for the particles with diameters of 15, 20, and 29 μm. The calculated temperature and speed of particles with diameters of 15, 20, and 29 μm were close to the experimental results for the LIP-mode operation. From the above comparison between the model calculations and experiments, the present model calculations are considered valid.

Figure 9 shows the calculated acceleration process of a particle with a diameter of 20 μm. In the model calculations, the particle speeds at $x = 0.1$ m were 631 m/s for the GAP-mode operation and 668 m/s for the LIP-mode operation. The difference between these speeds is only 27% of the difference in $u_{g,0}$ (gas flow speed at the CJ surface of the detonation) between the GAP and LIP operation modes. A particle was accelerated by the flow of fresh explosive gas from $x = -0.15$ m to $x = 0$. The gas flow speed of the fresh explosive gas was $u_{g,x<0} = 228$ m/s for the GAP-mode operation and $u_{g,x<0} = 110$ m/s for the LIP-mode operation. Due to this large difference in $u_{g,x<0}$ between the GAP and LIP operation modes, the calculated particle speeds at $x = 0$ were 157 m/s for the GAP-mode operation and 78 m/s for the LIP-mode operation. After the particle acceleration by the flow of fresh explosive gas, the particle is accelerated by the burned gas jet from $x = 0$ to $x = 0.1$ m. The increase of the particle speed between $x = 0$ and $x = 0.1$ m was 474 m/s for the GAP-mode operation and 590 m/s for the LIP-mode operation, and the difference in these values reaches 83% of the difference in $u_{g,0}$ between the GAP and LIP operation modes. That is, the increase of the particle speed due to the acceleration by the burned gas jet intensively reflected the difference in the gas flow speed at the CJ surface of the detonation. However, the difference in the increase of the particle speed due to the acceleration by the flow of fresh explosive gas reduced the difference in the particle speed at $x = 0.1$ m to only 27% of the difference in the gas flow speed at the CJ surface of the detonation.

Figure 10 shows the calculated heating process of a particle with a diameter of 20 μm. In the model calculations, the particle temperatures at $x = 0.1$ m were 1988 °C for the GAP-mode operation and 2973 °C for the LIP-mode operation. The difference in these values was 265% of the difference in the CJ temperature between the GAP and LIP operation modes. This large difference in the particle temperatures at $x = 0.1$ m was due to the large

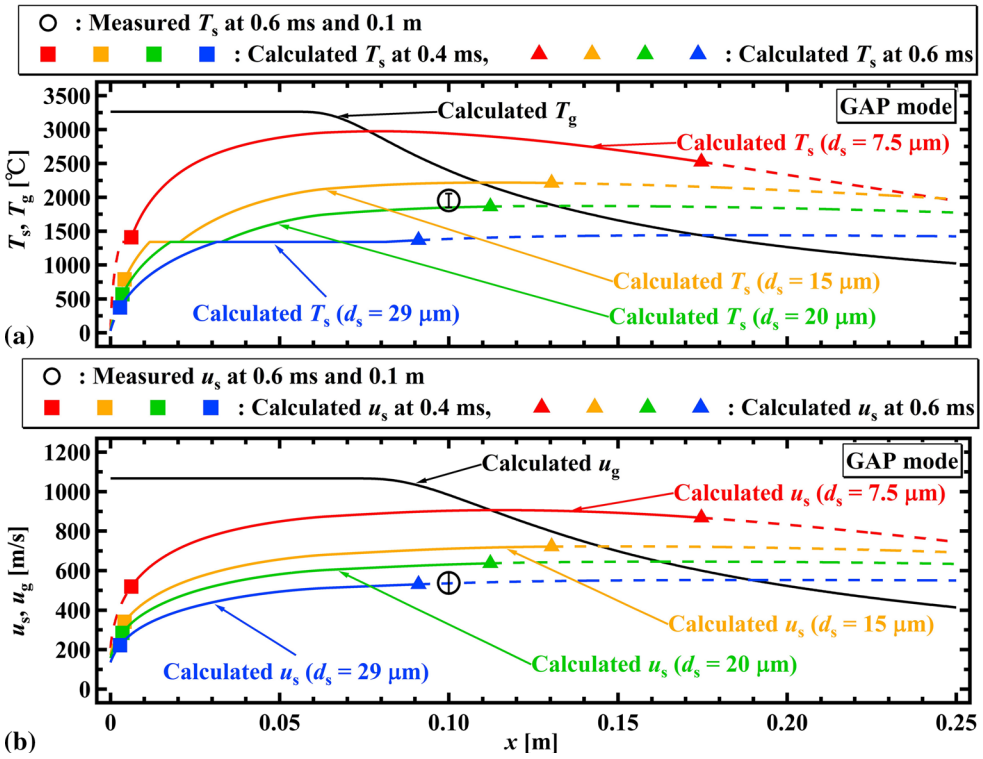

Fig. 7 Comparison of the calculation results for the GAP-mode operation with the experimental results of temperature (a) and speed (b)

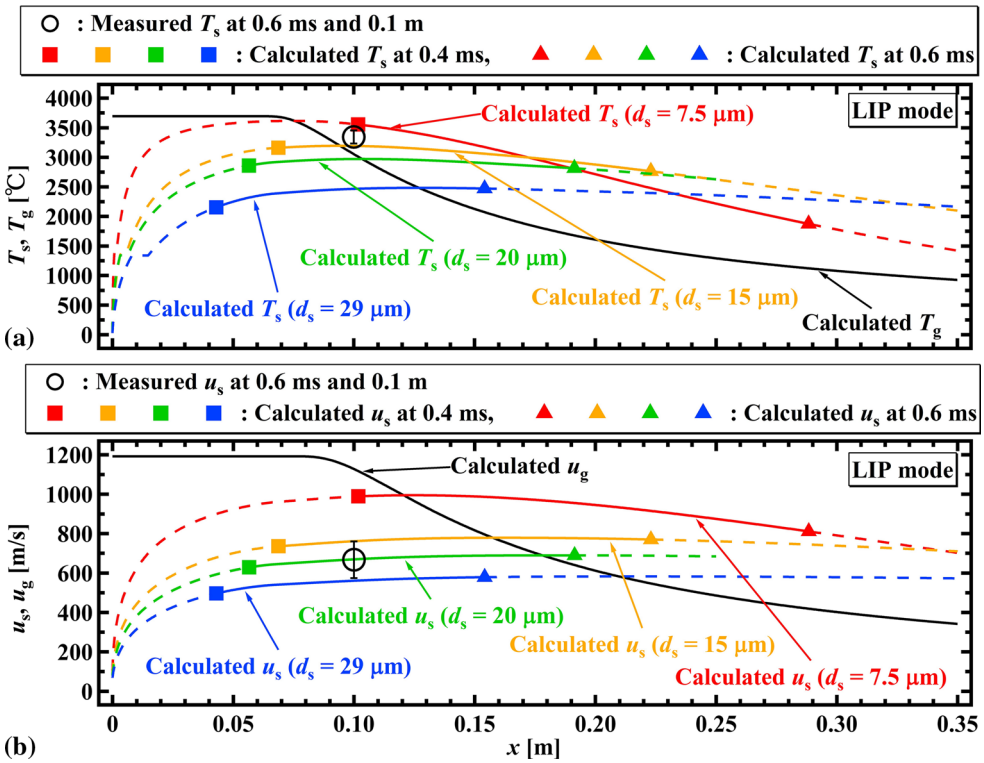

Fig. 8 Comparison of the calculation results for the LIP-mode operation with the experimental results of temperature (a) and speed (b)

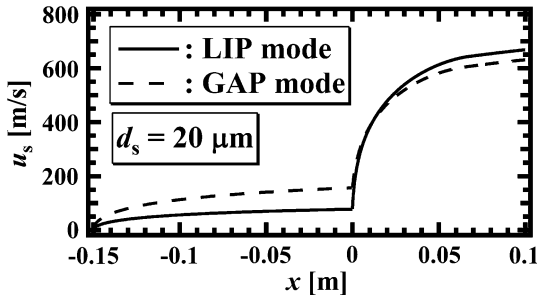

Fig. 9 Calculated acceleration process of a 20-μm particle

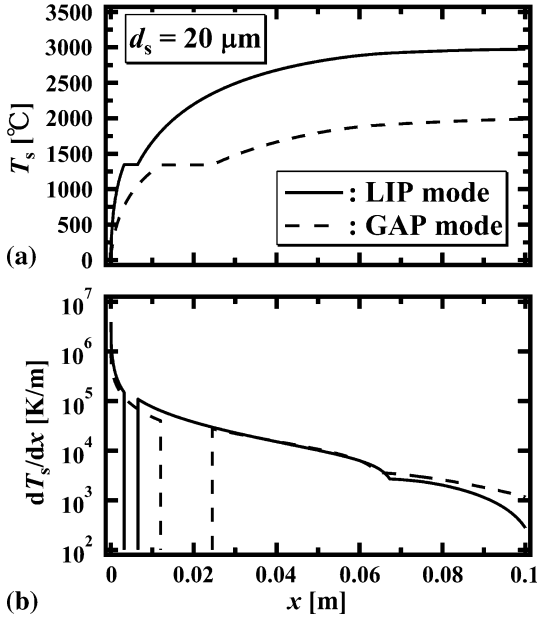

Fig. 10 Calculated temperature (a) and heating rate (b) in the heating process of a 20-μm particle

difference in dT_s/dx in the region $0 \le x < 0.02$ m, as shown in Fig. 10(b), where the regions in which $dT_s/dx = 0$ correspond to the particle fusion.

The origin of this large difference in dT_s/dx in the region $0 \le x < 0.02$ m is discussed. From Eq 4, dT_s/dx can be written as follows.

$$\frac{dT_s}{dx} = \frac{\pi d_s^2}{m_s c_s} \alpha \frac{1}{u_s} (T_g - T_s) \qquad \text{(Eq 28)}$$

Figure 11(a) shows the ratios of α, $1/u_s$, and $T_g - T_s$ between the LIP and GAP operation modes. As shown in Fig. 11(a), the value of $\alpha_{LIP}/\alpha_{GAP}$ was consistently in the range of 1.6-1.7, the value of $(1/u_s)_{LIP}/(1/u_s)_{GAP}$ was about 2 near the PDC exit and, after, rapidly became about unity, the value of $(T_g - T_s)_{LIP}/(T_g - T_s)_{GAP}$ was about unity near the PDC exit and gradually decreased from $x \approx 0.01$ m, and, finally, the product of $(T_g - T_s)_{LIP}/(T_g - T_s)_{GAP}$ and $\alpha_{LIP}/\alpha_{GAP}$ became about unity. From the above, it was determined that the origin of the large

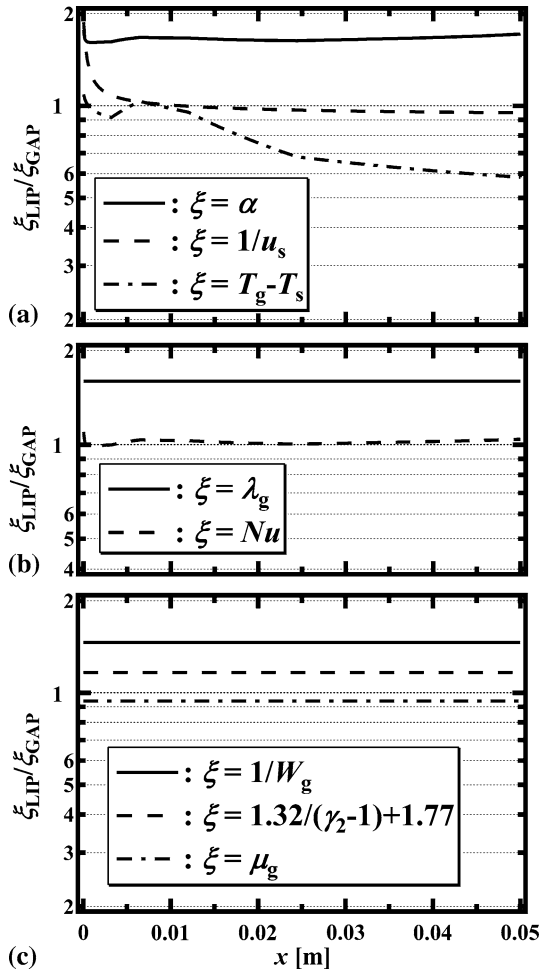

Fig. 11 Ratios of α, $1/u_s$, $T_g - T_s$ (a), λ_g, Nu (b), and $1/W_g$, $1.32/(\gamma_2 - 1) + 1.77$, μ_g (c) between the LIP and GAP modes

difference in dT_s/dx in the region $0 \le x < 0.02$ m was mainly the large value of $\alpha_{LIP}/\alpha_{GAP}$ in that region.

For further discussion of the origin of the large value of $\alpha_{LIP}/\alpha_{GAP}$ ($\alpha = \lambda_g Nu/d_s$), the ratios of λ_g and Nu between the LIP and GAP operation modes are shown in Fig. 11(b). As shown in Fig. 11(b), the value of $(\lambda_g)_{LIP}/(\lambda_g)_{GAP}$ was constant at about 1.6, and the value of Nu_{LIP}/Nu_{GAP} was constant at about unity. Accordingly, the origin of the large value of $\alpha_{LIP}/\alpha_{GAP}$ was the large value of $(\lambda_g)_{LIP}/(\lambda_g)_{GAP}$. In the present model calculations, the thermal conductivity λ_g was evaluated by using Eq 16. For further investigation, the ratios of $1/W_g$, $1.32/(\gamma_2 - 1) + 1.77$, and μ_g between the LIP and GAP operation modes are shown in Fig. 11(c). The values of the viscosity of gas μ_g were almost the same between the LIP and GAP operation modes. However, both $1/W_g$ and $1.32/(\gamma_2 - 1) + 1.77$ contributed to the large value of $(\lambda_g)_{LIP}/(\lambda_g)_{GAP}$. That is, both the average molar mass of the burned gas W_g and the effective specific-heat ratio of the burned gas γ_2 were larger for the GAP-mode operation than the LIP-mode operation. This was because the value of the mole fraction of argon, which is a monatomic

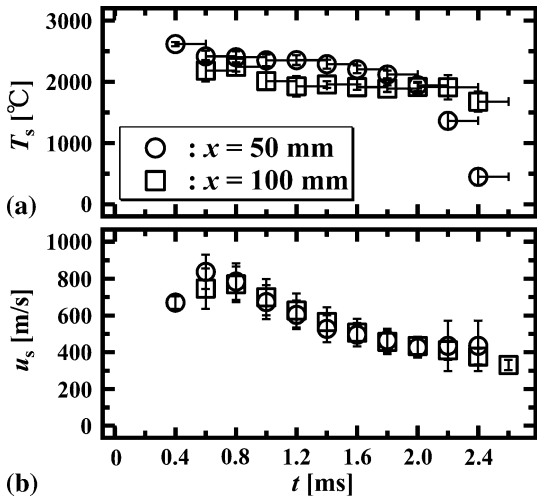

Fig. 12 Measured temperature (a) and speed (b) of the in-flight YSZ particles

molecule with a large molar mass, was large (54%) in the burned gas for the GAP-mode operation.

4. Thermal Spray of YSZ in the LIP Mode

It has been found that particles can be heated to a higher temperature in the LIP-mode operation than in the GAP-mode operation. Based on this, the ability of the developed LIP-mode PDC to spray ZrO_2-8 wt.% Y_2O_3 (YSZ), known as a high-melting-point ceramic, is examined.

4.1 Preliminary Experiments on Particle Temperature and Speed

All experiments relevant to YSZ described in section 4.1 and 4.2 were conducted with the addition of an extension barrel, whose inner diameter was 10 mm and length was 300 mm, on the exit of the PDC shown in Fig. 2. Preceding the thermal spray experiment on YSZ, the temperature and speed of in-flight YSZ particles were measured by using SprayWatch 2i, where the center of the field of view was set 50 or 100 mm from the exit of the extension barrel for determining the appropriate stand-off distance of the thermal spray experiment. The reason why 50 and 100 mm were chosen was that, as shown in Fig. 8(a), the temperature of the burned gas jet began to decrease at about 70 mm from the gun exit, decreased to about 3000 °C at about 100 mm, and then decreased lower than the melting point of YSZ further than 100 mm. The operation conditions of the PDC are summarized in Table 2. The PDC was operated at 150 Hz for 20 s. The YSZ particles were supplied into the PDC at the rate of 10 g/min. The temperature and speed of the in-flight particles were measured without a substrate to be sprayed.

Figure 12 shows the measured temperature and speed of the YSZ particles, where x denotes the distance from the exit of the extension barrel. As a result, the temperature of the YSZ particles measured at $x = 50$ mm was higher than that at $x = 100$ mm, although the speeds of the YSZ particles were almost the same in both cases. Based on the above results, the stand-off distance of the thermal spray experiment was determined to be 50 mm.

Table 2 Operation conditions of the LIP-mode PDC for experiments on YSZ particles

Supply pressure of C_2H_4 and O_2, MPa	0.60
Supply rate of C_2H_4, slm	168
Supply rate of O_2, slm	402
Composition of explosive gas	$1.25C_2H_4 + 3O_2$
Temperature at CJ surface, K	3994
Pressure at CJ surface, MPa	3.657
Gas speed at CJ surface relative to the unburned gas, m/s	1142
Mass of injected water per cycle, mg	28

4.2 Thermal Spray Experiment

In the thermal spray experiment, a flat substrate of SUS304, with dimensions of 50 mm × 50 mm, was set at $x = 50$ mm, where both the PDC and substrate were fixed spatially. The surface of the substrate was grit blasted using aluminum oxide powder prior to the coating process, and the arithmetic mean roughness R_a of the roughened surface was $R_a = 2.42 \pm 0.18$ μm, which was measured by using a "TOKYO SEIMITSU, HANDYSURF E-MD-S180A." The conditions of the thermal spray experiment were the same as those of the experiments described in section 4.1.

Figure 13 shows the YSZ coating deposited in the present experiment. The thickness of the coating was about 200 μm at the center. The porosity of the coating was about 1.4%, which was determined by binarizing the electron micrograph of the cross section of the coating shown in Fig. 13(c). This value is close to the result of the thermal spray experiment using HFPD (Ref 54). Because the porosity of YSZ coatings deposited for SOFC by using plasma spray is 2.1-6.7% (Ref 36, 55), it is concluded that the YSZ coating deposited in the present experiment is dense. In the present thermal spray experiment, the measured mass increase of the sprayed substrate was 0.09 g, corresponding to the utilization ratio of the YSZ powder of 0.027 on the assumption of stable constant powder feeding rate of 10 g/min. On the other hand, the time width during which hot particles were observable by their self-emission was 1.2 ms per cycle as stated earlier, although the period of one cycle was 6.67 ms (1/150 s). Therefore, the duty ratio of the pulse detonation thermal spray is evaluated to be 0.18. Accordingly, the utilization ratio of the YSZ powder was 15% of the duty ratio of the pulse detonation thermal spray. That is, only a small portion of the supplied powder suitably heated and accelerated for deposition formed the coating. This may be one of the reasons why the YSZ coating deposited in the present experiment is dense.

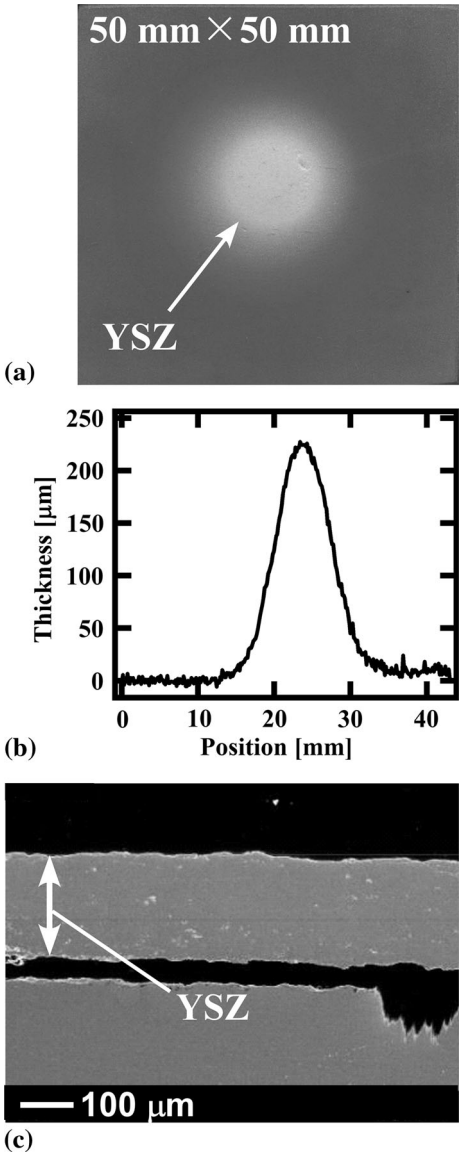

Fig. 13 YSZ-coated substrate (a), coating thickness (b), and cross-sectional photograph of the YSZ coating by a scanning electron microscope (c)

5. Conclusions

Two types of PDCs were prepared, one operated in the GAP mode and the other in the LIP mode, and operated at 150 Hz. In both cases, CoNiCrAlY particles were supplied into the combustor, and the temperature and speed of the in-flight particles were measured. As a result, both the temperature and speed of the particles supplied into the combustor operated in the LIP mode were higher than those of the particles supplied into the combustor operated in the GAP mode. This was because the chemical compositions of the explosive gas mixtures were different between the LIP and GAP modes, and the difference in the heating and acceleration processes in these two modes was clarified by using simple model calculations. Furthermore, a thermal spray experiment was conducted using YSZ (8 wt.% Y_2O_3-ZrO_2) as an example of a high-melting-point material and a dense coating was successfully deposited.

Acknowledgment

This work was supported by KAKENHI 26289323 and JKA 25-148.

References

1. W. Fickett and W.C. Davis, *Detonation*, University of California Press, Berkeley, 1979
2. J.H.S. Lee, *The Detonation Phenomenon*, Cambridge University Press, New York, 2008
3. J.A. Nicholls, H.R. Wilkinson, and R.B. Morrison, Intermittent Detonation as a Thrust-Producing Mechanism, *Jet Propul.*, 1957, **27**(5), p 534-541
4. F. Schauer, J. Stutrud, and R. Bradley, Detonation Initiation Studies and Performance Results for Pulsed Detonation Engine, *AIAA Paper* 2001-1129, 2001
5. W.H. Heiser and D.T. Pratt, Thermodynamic Cycle Analysis of Pulse Detonation Engines, *J. Propul. Power*, 2002, **18**(1), p 68-76
6. G.D. Roy, S.M. Frolov, A.A. Borisov, and D.W. Netzer, Pulse Detonation Propulsion: Challenges, Current Status, and Future Perspective, *Progr. Energy Combust. Sci.*, 2004, **30**(6), p 545-672
7. T. Endo, J. Kasahara, A. Matsuo, K. Inaba, S. Sato, and T. Fujiwara, Pressure History at the Thrust Wall of a Simplified Pulse Detonation Engine, *AIAA J.*, 2004, **42**(9), p 1921-1930
8. T. Endo, T. Yatsufusa, S. Taki, A. Matsuo, K. Inaba, and J. Kasahara, Homogeneous-Dilution Model of Partially Fueled Simplified Pulse Detonation Engines, *J. Propul. Power*, 2007, **23**(5), p 1033-1041
9. T. Endo, T. Yatsufusa, S. Taki, and J. Kasahara, Thermodynamic Analysis of the Performance of a Pulse Detonation Turbine Engine, *Sci. Tech. Energ. Mater.*, 2004, **65**(4), p 103-110 (in Japanese)
10. T. Takahashi, A. Mitsunobu, Y. Ogawa, S. Kato, H. Yokoyama, A. Susa, and T. Endo, Experiments on Energy Balance and Thermal Efficiency of Pulse Detonation Turbine Engine, *Sci. Tech. Energ. Mater.*, 2012, **73**(6), p 181-187
11. R.C. Tucker, Jr., Thermal spray coatings, *ASM Handbook*, Vol 5, Surface Engineering , C.M. Cotell, J.A. Sprague, and F.A. Smidt, Jr., Ed., ASM International, Materials Park, 1994, p 497-509
12. O. Knotek, Thermal Spraying and Detonation Gun Processes, *Handbook of Hard Coatings*, R.F. Bunshah, Ed., Noyes Publications, Park Ridge, 2001, p 77-107
13. P. Fauchais, A. Vardelle, and B. Dussoubs, Quo Vadis Thermal Spraying?, *J. Thermal Spray Technol.*, 2001, **10**(1), p 44-66
14. A.S.M. Ang, N. Sanpo, M.L. Sesso, S.Y. Kim, and C.C. Berndt, Thermal Spray Maps: Material Genomics of Processing Technologies, *J. Thermal Spray Technol.*, 2013, **22**(7), p 1170-1183
15. Y.A. Kharlamov, Detonation Spraying of Protective Coatings, *Mater. Sci. Eng.*, 1987, **93**, p 1-37
16. E.A. Astakhov, Controlling the Properties of Detonation-Sprayed Coatings: Major Aspects, *Powder Metall. Met. Ceram.*, 2008, **47**(1–2), p 70-79
17. Yu.A. Nikolaev, A.A. Vasil'ev, and B.Yu. Ul'yanitskii, Gas Detonation and Its Application in Engineering and Technologies (Review), *Combust. Expl. Shock Waves*, 2003, **39**(4), p 382-410
18. A. Fujii, T. Akitomo, T. Okamoto, A. Susa, T. Endo, and S. Taki, High-Frequency Operation of Pulse Detonation Combustor in Valveless Mode, *Proceeding of the 6th Asian-Pacific Conf. on Aerospace Technol. and Sci. (CD-ROM)*, Nov. 15-19, 2009 (Huangshan, China)
19. T. Endo, Thermal Spray by Pulsed Detonations, *2013 International Workshop on Detonation for Propulsion (USB memory)*, July 26-28, 2013 (Tainan, Taiwan)

20. K. Matsuoka, T. Mukai, and T. Endo, Development of a Liquid-Purge Method for High-Frequency Operation of Pulse Detonation Combustor, *Combust. Sci. Technol.*, 2015, **187**(5), p 747-764
21. P. Saravanan, V. Selvarajan, D.S. Rao, S.V. Joshi, and G. Sundararajan, Influence of Process Variables on the Quality of Detonation Gun Sprayed Alumina Coatings, *Surf. Coat. Technol.*, 2000, **123**(1), p 44-54
22. H. Du, W. Hua, J. Liu, J. Gong, C. Sun, and L. Wen, Influence of Process Variables on the Qualities of Detonation Gun Sprayed WC-Co Coatings, *Mater. Sci. Eng. A*, 2005, **408**(1–2), p 202-210
23. C. Henkes and H. Olivier, Flow Characterization of a Detonation Gun Facility and First Coating Experiments, *J. Thermal Spray Technol.*, 2014, **23**(5), p 795-808
24. B.J. Gill, Super D-Gun, *Aircraft Eng.*, 1990, **62**(8), p 10-14
25. K. Niemi, P. Vuoristo, and T. Mäntylä, Properties of Alumina-Based Coatings Deposited by Plasma Spray and Detonation Gun Spray Processes, *J. Thermal Spray Technol.*, 1994, **3**(2), p 199-203 (Errata **3**(3), p 242)
26. I. Fagoaga, G. Barykin, J. de Juan, T. Soroa, and C. Vaquero, The High Frequency Pulse Detonation (HFPD) Spray Process, *Thermal Spray 1999: United Thermal Spray Conference*, Tagungsband Conference Proceedings, E. Lugscheider and R.A. Kammer, Ed., March 17-19, 1999 (Düsseldorf, Germany), DVS Deutscher Verband für Schweißen, 1999, p 282-287
27. M. Parco, G. Barykin, I. Fagoaga, and C. Vaquero, Development of Wear Resistant Ceramic Coatings by HFPD, *Thermal Spray 2008: Thermal Spray Crossing Borders*, E. Lugscheider, Ed., June 2-4, 2008 (Maastricht, The Netherlands), ASM International, 2008, p 130-134
28. F.J. Belzunce, V. Higuera, and S. Poveda, High Temperature Oxidation of HFPD Thermal-Sprayed MCrAlY Coatings, *Mater. Sci. Eng. A*, 2001, **297**(1–2), p 162-167
29. V.H. Hidalgo, F.J.B. Varela, and J.R. López, Cyclic High Temperature Oxidation of HFPD Thermal Sprayed CoNiCrAlY Coatings Under Simulated Gas Turbine and Furnace Environments, *Surf. Eng.*, 2006, **22**(4), p 277-282
30. M.C. Mayoral, J.M. Andrés, M.T. Bona, V. Higuera, and F.J. Belzunce, Yttria Stabilized Zirconia Corrosion Destabilization Followed by Raman Mapping, *Surf. Coat. Technol.*, 2008, **202**(21), p 5210-5216
31. F. Mubarok, S. Armada, I. Fagoaga, and N. Espallargas, Thermally Sprayed SiC Coatings for Offshore Wind Turbine Bearing Applications, *J. Thermal Spray Technol.*, 2013, **22**(8), p 1303-1309
32. V. Higuera, F.J. Belzunce, and J. Riba, Influence of the Thermal-Spray Procedure on the Properties of a CoNiCrAlY Coating, *Surf. Coat. Technol.*, 2006, **200**(18–19), p 5550-5556
33. V. Higuera, F.J. Belzunce, A. Carriles, and S. Poveda, Influence of the Thermal-Spray Procedure on the Properties of a Nickel-Chromium Coating, *J. Mater. Sci.*, 2002, **37**(3), p 649-654
34. F.J. Belzunce, V. Higuera, S. Poveda, and A. Carriles, High Temperature Oxidation of HFPD Thermal-Sprayed MCrAlY Coatings in Simulated Gas Turbine Environments, *J. Thermal Spray Technol.*, 2002, **11**(4), p 461-467
35. K. Tani and H. Nakahira, Status of Thermal Spray Technology in Japan, *J. Thermal Spray Technol.*, 1992, **1**(4), p 333-339
36. D. Soysal, J. Arnold, P. Szabo, R. Henne, and S.A. Ansar, Thermal Plasma Spraying Applied on Solid Oxide Fuel Cells, *J. Thermal Spray Technol.*, 2013, **22**(5), p 588-598
37. Cobalt Nickel Chromium Aluminum Yttrium (CoNiCrAlY) Thermal Spray Powders, *Material Product Data Sheet*, DSMTS-0092.5-CoNiCrAlY Powders, Oerlikon Metco, 2014
38. Y. Hirayama, T. Matsumoto, H. Motomura, and S. Ono, Casting Method for Surface Coating, *Published Unexamined Patent Application*, P2004-74202A, Japan Patent Office, 2004 (in Japanese)
39. 8% Yttria Stabilized Zirconia Agglomerated and HOSP Thermal Spray Powders, *Material Product Data Sheet*, DSMTS-0001.5-HOSP 8% YsZ Powders, Oerlikon Metco, 2014
40. W.C. Reynolds, The Element Potential Method for Chemical Equilibrium Analysis: Implementation in the Interactive Program STANJAN, Version 3, *Technical Rept.*, Dept. of Mechanical Engineering, Stanford Univ., 1986
41. A. Haider and O. Levenspiel, Drag Coefficient and Terminal Velocity of Spherical and Nonspherical Particles, *Powder Technol.*, 1989, **58**(1), p 63-70
42. D.J. Carlson and R.F. Hoglund, Particle Drag and Heat Transfer in Rocket Nozzles, *AIAA J.*, 1964, **2**(11), p 1980-1984
43. S. Whitaker, Forced Convection Heat Transfer Correlations for Flow in Pipes, Past Flat Plates, Single Cylinders, Single Spheres, and for Flow in Packed Beds and Tube Bundles, *AIChE J.*, 1972, **18**(2), p 361-371
44. C. Henkes and H. Olivier, Particle Acceleration in a High Enthalpy Nozzle Flow with a Modified Detonation Gun, *J. Thermal Spray Technol.*, 2014, **23**(4), p 625-640
45. L.L. Kavanau and R.M. Drake, Jr., Heat Transfer from Spheres to a Rarefied Gas in Subsonic Flow, *Technical Rept.*, HE-150-108, Univ. of California, 1953
46. R.B. Bird, W.E. Stewart, and E.N. Lightfoot, *Transport Phenomena, Sec. 1.4*, 2nd ed., Wiley, New York, 2002
47. C.K. Law, *Combustion Physics, Ch. 4*, Cambridge University Press, New York, 2006
48. R.S. Brokaw, Predicting Transport Properties of Dilute Gases, *Ind. Eng. Chem. Process Des. Dev.*, 1969, **8**(2), p 240-253
49. B.E. Poling, J.M. Prausnitz, and J.P. O'Connell, *The Properties of Gases and Liquids*, 5th ed., McGraw-Hill, New York, 2001, p 10.3
50. T. Fujii and T. Takahashi, Estimation of Thermophysical Properties of Coating Layers for Gas Turbine Hot Parts—Part 1: Measurement of Thermophysical Properties of Coating Layers and Superalloy, and Comparison between Virgin and Aged Material—, *CRIEPI REPORT*, W97017, Central Research Institute of Electric Power Industry, 1998 (in Japanese)
51. E. Romeo, C. Royo, and A. Monzón, Improved Explicit Equations for Estimation of the Friction Factor in Rough and Smooth Pipes, *Chem. Eng. J.*, 2002, **86**(3), p 369-374
52. P.O. Witze, Centerline Velocity Decay of Compressible Free Jets, *AIAA J.*, 1974, **12**(4), p 417-418
53. G. Kleinstein, Mixing in Turbulent Axially Symmetric Free Jets, *J. Spacecr.*, 1964, **1**(4), p 403-408
54. I. Fagoaga, M. Parco, G. Barykin, C. Vaquero, and J. de Juan, Development of Zirconia Coatings by HFPD, *Thermal Spray 2006: International Thermal Spray Conference*, B.R. Marple, M.M. Hyland, Y.-C. Lau, R.S. Lima, and J. Voyer, Ed., May 15-18, 2006 (Seattle, USA), ASM International, 2006, p 551-556
55. A.R. Nicoll and A. Salito, The Potential of Plasma Spraying for the Deposition of Coatings on SOFC Components, *Solid State Ionics*, 1992, **52**(1–3), p 269-275